Mon. Not. R. Astron. Soc. **000**, 1–11 (2014) Printed 21 August 2014 (MN LATEX style file v2.2)

On Spectral Evolution and Temporal Binning in Gamma-Ray Bursts

J. Michael Burgess[1,2⋆]
[1] *The Oskar Klein Centre for Cosmoparticle Physics, AlbaNova, SE-106 91 Stockholm, Sweden*
[2] *Department of Physics, KTH Royal Institute of Technology, AlbaNova, SE-106 91 Stockholm, Sweden*

arXiv:1408.3973v2 [astro-ph.HE] 20 Aug 2014

Accepted XXXX December XX. Received XXXX December XX; in original form XXXX October XX

ABSTRACT

The understanding of the prompt γ-ray spectra of gamma-ray bursts (GRBs) is of great importance to correctly interpreting the physical mechanisms that produce the underlying event as well as the structure of the relativistic jet from which the emission emanates. Time-resolved analysis of these spectra is the main method of extracting information from the data. In this work, several techniques for temporal binning of GRB spectra are examined to understand the systematics associated with each with the goal of finding the best method(s) to bin lightcurves for analysis. The following binning methods are examined: constant cadence (CC), Bayesian blocks (BB), signal-to-noise (S/N) and Knuth bins (KB). I find that both the KB and BB methods reconstruct the intrinsic spectral evolution accurately while the S/N method fails in most cases. The CC method is accurate when the cadence is not too coarse but does not necessarily bin the data based on the true source variability. Additionally, the integrated pulse properties are investigated and compared to the time-resolved properties. If intrinsic spectral evolution is present then the integrated properties are not useful in identifying physical and cosmological properties of GRBs without knowing the physical emission mechanism and its evolution.

Key words: (stars:) gamma ray bursts – methods: data analysis

1 INTRODUCTION

Spectral evolution has long been studied in the context of GRBs (Golenetskii et al. 1983; Liang & Kargatis 1996; Crider et al. 1998; Norris et al. 1986; Burgess et al. 2014; Guiriec et al. 2010). While the shape of the spectrum can aid in identifying the type of emission mechanism occurring in the jet, spectral evolution can elucidate the temporal evolution of the density, magnetic field, and structure of the jet. The unprecedented spectral and temporal resolution of the *Fermi* Gamma-ray Burst Monitor (GBM) (Meegan et al. 2009) allows for detailed observations of the evolution of GRB spectra. It is therefore important to evaluate the ability of GBM to measure the intrinsic spectral evolution of a GRB.

To reconstruct the spectral evolution of GRBs in the data, the observed lightcurve must be binned in time. Due to the way photons are detected by GBM, their true energy is not known and the shape of the spectrum can only be ascertained after the data have been binned in time and folded through the instrument's detector response matrices (DRMs). Therefore, it is impossible to bin the data in time based on the intrinsic spectral evolution a priori. Binning must then be based upon a balance between having enough signal to accurately fit the spectrum and having a fine enough time-resolution to detected the intrinsic changes in the spectrum over time. Hence, several methods to bin the data in GRB spectral analysis have been developed. In this work, these methods are investigated to evaluate their ability to accurately reconstruct the intrinsic spectral evolution in GRBs.

Since it is impossible to know the intrinsic spectral evolution in a GRB, this investigation requires a set of simulated GRBs with known intrinsic spectral evolution. This is achieved via a simulation code that can map an evolving photon model into GBM time-tagged event (TTE) data which can then be analyzed like real source data. These simulations also afford the ability to examine the integrated properties of GRB spectra as compared to the known evolution of the spectra. With the integrated properties being important to using GRBs as cosmological tools, this investigation can provide insights to the power of these properties to be indicative of the physical properties of the source.

This article is organized in the following way: Section 2

⋆ E-mail: jamesb@kth.se (JMB)

© 2014 RAS

provides a description of the simulation method used to construct the control set of GRB pulses, Section 3 introduces the binning methods to be investigated, Section 4 describes the simulated data set that will be binned and analyzed, and Section 5 investigates the results of the study for both spectral evolution and the integrated properties of the simulated GRBs.

2 GBM TTE SIMULATOR

In order to assess the ability of the various binning methods to accurately reconstruct the spectral evolution of GRB emission, it is imperative to create a control set of simulated GRB data with known spectral evolution. The simulated data must meet two requirements to be of use in this study:

- the freedom to rebin the data to arbitrary binnings
- and data must be folded through GBM DRMs to mimic the response of the instrument.

Achieving these requirements is not possible with the two widely used analysis software packages for GRB spectral analysis; XSPEC Arnaud (1996) and RMFIT[1]. Therefore, a simulator was designed that can generate GBM TTE data for any photon model that is a function of time and energy.

First, a spectral shape such as the Band function (Band et al. 1993) is chosen as the primary shape to be simulated. The spectral parameters are given as a function of time yielding a function $\mathcal{F}_{\rm evo}(\varepsilon, t_{\rm a})$ [phts s^{-1} cm^{-2}] that is the equation for the simulated lightcurve. Here, ε is the photon energy and $t_{\rm a}$ is the arrival time of the photon. This equation is then numerically integrated over the duration of the emission to obtain the bolometric lightcurve so that the number of photons to be generated is known. From the bolometric lightcurve, time-tags for the arrival time of photons are generated using a non-homogeneous Poisson generator. This method randomly selects arrival times via an inverted Poisson distribution and then thins the number of time-tags to the shape of the bolometric lightcurve via an acceptance-rejection sampler. The time-tags will ultimately be the TTE time-tags in the generated data file.

Once the $t_{\rm a}$'s of all photons are generated, they are input into $\mathcal{F}_{\rm evo}$ projecting the function into being the energy distribution of photons at $t = t_{\rm a}$. This energy distribution is treated as a probability distribution from which photon energies are randomly selected via a second acceptance-rejection sampler. After all photons have a time and energy tag associated with them, the energies must be converted to GBM pulse-height analysis (PHA) channel. This is performed by selecting a GBM DRM for each detector that will have a simulated data set. The two types of detectors on GBM are Sodium Iodide (NaI) for the energy range 8-2000 keV and Bismuth Germanate (BGO) for the energy range 300-40000 keV. The DRMs map photon energy into PHA channel and encode the physical interactions that occur during photon detection inside the crystals. Each photon energy row of the response matrix is converted to a probability distribution in PHA channel space via dividing by the geometric area of the detector. The geometric area is calculated by computing the projected area of the detector at the proper incident angle for the simulated source. This method properly takes into account the possibility that an incident photon can deposit more than one count in the detector as a result of multiple scattering.

A homogeneous Poisson background is superimposed on the source data using the same technique as described above except that the photon spectrum of the background is assumed to be a simple power law. The index of the power law used for all simulations in this work is -1.4 and was chosen by fitting the low-energy portion of several GBM background intervals. However, it was checked that changing the value of this photon index did not affect the fit results of the source spectrum. This indicates that the background subtraction technique used in RMFIT is correctly removing the background from the source when the background is fit properly.

Once the detector counts are all tagged in channel number and time, they are saved in the standard GBM TTE FITS file format and can be analyzed with RMFIT as if they were real data. The TTE data can then be freely rebinned in time to test various binning methods.

3 BINNING METHODS

In this section, the various methods for creating time bins for spectral analysis of GRBs are described. The time evolution of spectral parameters is key to unraveling the complex emission mechanisms and jet dynamics in GRBs. Yet, there is no standard method for binning the data and one is typically selected based upon the desired purposes of the experiment. Ideally, the method chosen should be objective. All these methods share a common drawback in that they cannot bin the data in time based on the spectral evolution of the GRB. Attempts have been made to do this (Guiriec et al. 2013) but will not be investigated here.

3.1 Constant Cadence

The simplest method for binning the data is by choosing a constant cadence (CC) where the time bins are uniform throughout the duration of the GRB. The method is objective in how the variability of the burst is treated. For example, once a bin width (ΔT) and start time (T_0) are selected, the choice of bins is completely determined. Moreover, the choice of binning does not depend on the flux history or energy distribution of the burst. For this work, three cadences are selected to bin the data: $\Delta T = 5.0s, 1.0s, 0.5s$ denoted as $\rm CC_5$, $\rm CC_1$, $\rm CC_{0.5}$ respectively.

Drawbacks of this method are that the choice of one bin width for the duration of the burst, while objective, neglects the fact that the flux history and spectral shape may change slower or faster than the chosen cadence.

3.2 Bayesian Blocks

Bayesian blocks (BBs) (Scargle et al. 2013) are time bins chosen such that each bin is consistent with a constant Poisson rate. This is done by algorithmically subdividing the flux history of the GRB lightcurve and comparing the likelihood of the distribution of the count rate of each bin to being

[1] http://fermi.gsfc.nasa.gov/ssc/data/analysis/rmfit/

piecewise constant or constant. Time bins selected in this way will have a variable width and variable signal-to-noise ratio. The selection of the bins will reflect the true variability of the data which is advantageous for studying changes in flux.

The method does not insure that there is adequate signal in the bins to make an accurate spectral fit. This is because it considers fluctuations in the background on equal footing with the source. It is therefore beneficial that the data have a somewhat constant background or that the source be much more intense than the background.

3.3 Knuth Bins

Similar to BBs, the Knuth binning (KB) method (Knuth 2006) seeks to find the optimal binning based on the data alone using the assumption that the data are best described by a piecewise constant model. The method of KB differs by removing the assumption that prior information is known about the intrinsic density distribution of the bins and instead uses a Bayesian method that assumes little to no information about the prior distribution and that the bins all have equal width. The method seeks to find the simplest model that describes the variability of the data. In this sense, the method will not find the short duration features found by BBs but will have more counts or a greater signal-to-noise ratio over the duration of the burst.

3.4 Signal to Noise

When performing spectral analysis, it is necessary to have enough counts above background in the data to fit the spectrum with high significance. A way of guaranteeing that the ratio of signal counts to background counts remains constant is by defining bins with a given signal to noise ratio. To achieve this a background must be selected in the data. Starting from T_0, source and background are accumulated until the desired ratio is achieved. Herein, the signal to noise ratio is chosen to be 50 which is a slightly higher than what is used in the GBM spectral catalogs Goldstein et al. (2012). This results in varied bin width. Bins having high signal counts are narrow and those with a low signal flux are wide. While the bins will have uniform signal-to-noise ratios, the method completely neglects spectral evolution and the intrinsic flux history of the GRB. This neglect occurs in the sense that the method does not look back as it marches forward and bins the data and therefore arbitrarily combines bins with intrinsically different Poisson rates. Therefore, the method has change points that are a function of both the flux and the chosen T_0.

4 SIMULATION DATA SET

In order to examine the effects of various binning methods on reconstructing the intrinsic spectral evolution of GRBs, a set of simulated GRB data was created. This set consists of single pulses which can be viewed as the building blocks of more complex lightcurves. The spectrum chosen as the basis for the simulations is the common Band function; ubiquitous in the spectral analysis of GRBs. The Band function is a smoothly broken power law with a fixed curvature. It is

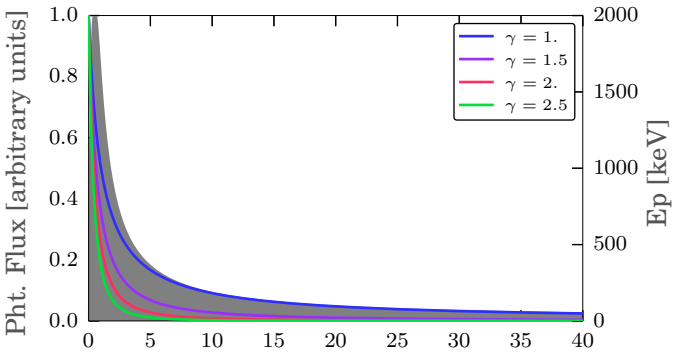

Figure 1. The intrinsic properties of the simulated datasets. The pulse profile is shown in *grey* and the different evolutions of $E_{\rm p}$ are super-imposed on the flux history.

parameterized by its low and high-energy spectral indices, α and β respectively, as well as its νF_ν peak energy, $E_{\rm p}$. The temporal evolution of the Band function's parameters have been studied in great detail in search for their physical connection to the outflow. Herein, the evolution of $E_{\rm p}$ is the focus of the investigation. One of the most common found evolutionary patterns of $E_{\rm p}$ is the so-called hard-to-soft evolution where $E_{\rm p}$ evolves from high to low energies over the duration of the GRB (Band 1997). Due to its commonality, hard-to-soft evolution will be the chosen form for these simulations and approximated as a power law in time:

$$E_{\rm p}\,(t) \;=\; E_0(t+1)^{-\gamma}. \qquad (1)$$

Here, γ is the decay index of $E_{\rm p}$ and four values are simulated: 1, 1.5, 2, and 2.5. For this study, E_0 is chosen to be 2 MeV.

To approximate a typical GRB, the amplitude of the Band function is evolved using the so-called KRL pulse shape given by Kocevski, Ryde & Liang (2003). Since the photon flux is modified by the value of $E_{\rm p}$ and the pulse shape should be the same for different values of γ, the amplitude is renormalized so that only the value the KRL pulse shape determines the flux. This insures that all simulated datasets have the same photon flux which is important when calculating the S/N and BB binnings. This introduces an artificial hardness-intensity correlation but does not affect the investigation here. The value of β is held fixed at its typically observed value of -2.2 for all simulated data. However, for each value of γ, a fixed value of α is chosen from set -1, 0, and 1. Therefore, there are 12 sets of simulated data in total. With all the parameters specified, the function $\mathcal{F}_{\rm evo}$ is completely defined and appears as shown in Figures 1 and 2.

For each combination of γ and α, three TTE files are generated (see Figure 3); two NaI files and one BGO file. The GRB pulses are all given a duration of 40 seconds with a super-imposed background of 80 seconds. The DRMs used to make the TTE files come from the detection of GRB 110721A (Axelsson et al. 2012) and were chosen such that the source angles to the detector normal are all less than 60°.

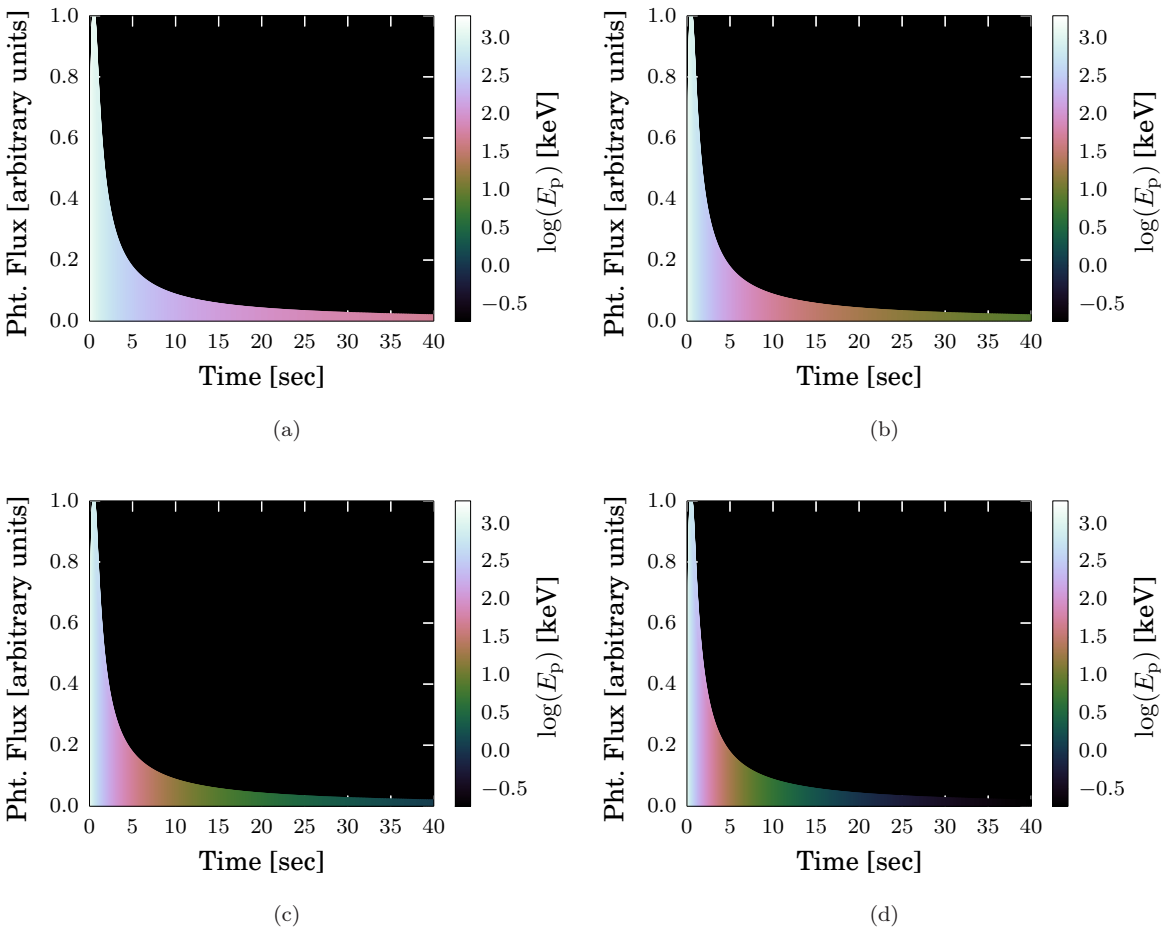

Figure 2. Illustrating the evolution of E_p as a function of the flux history for each choice of γ =1(a), 1.5(b). 2(c), 2.5(d).

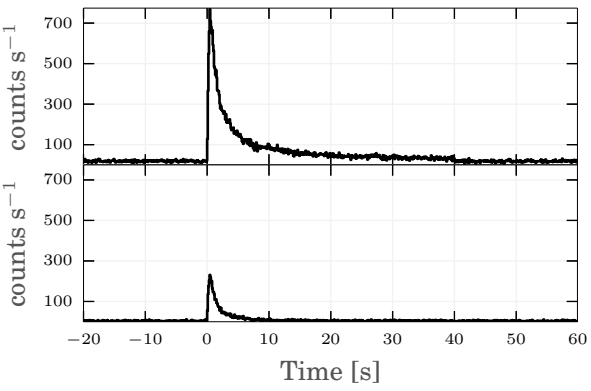

Figure 3. Example NaI (*top*) and BGO (*bottom*) TTE lightcurves generated from $\mathcal{F}_{\rm evo}$. The parameters used to generate this simulation are $\gamma = 1.$ and $\alpha = -1$. The background is a 0-order polynomial in time and is distributed in photon number as a power law with spectral index -1.4.

5 INVESTIGATING SPECTRAL EVOLUTION

5.1 Analysis Method

Each data set is temporally binned via the methods described in Section 3 (see Figure 4). For both the BB and KB methods the data were binned with the routines of the AstroML software library (VanderPlas et al. 2012).The backgrounds in each are fit with a constant background. The signal region of the pulse is selected and each time bin is fit with the Band function. Near the tail of the GRB, the weak flux causes some fits to fail and those time bins are excluded from the study. The photon flux and energy flux F_ν for each fit is calculated by integrating the model over the full bandpass.

5.2 Integrated Pulse Properties

The integrated E_p is a commonly investigated property of GRBs. Its correlation with the total F_ν has been used to relate GRBs to cosmological properties (Ghirlanda, Ghisellini & Lazzati 2004; Amati 2003; Ghirlanda, Ghisellini & Firmani 2005). It is important to understand the relevance of the integrated E_p to its time evolution with a GRB. In Figure 5, the integrated E_p is plotted against its evolution. Clearly, the integrated E_p is

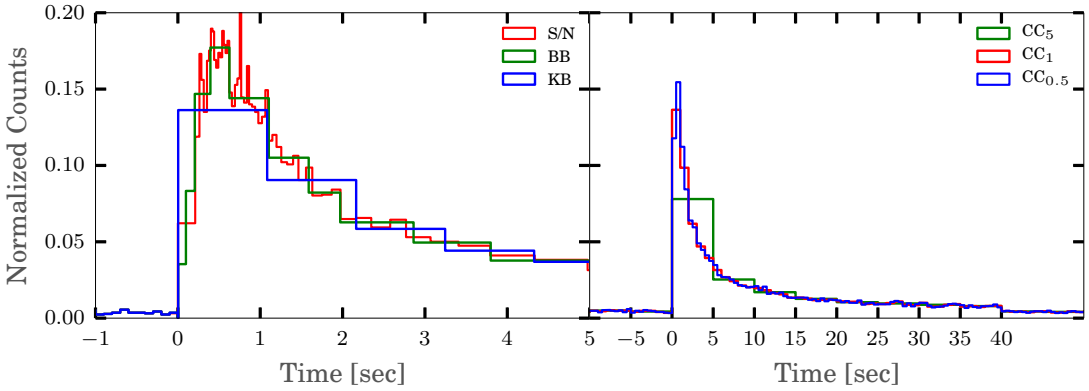

Figure 4. The temporal binning of the lightcurves with the above listed methods. The lightcurves have been normalized so they can be directly compared. The KB method does not resolve the shape of the peak as well as the BB method.

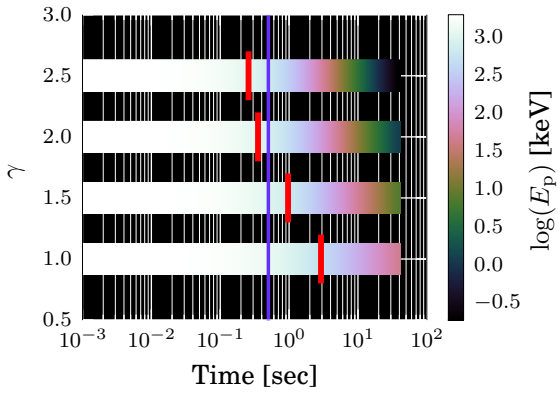

Figure 5. The fitted of $E_{\rm p}$ found by fitting the integrated spectrum (*red*) is super-imposed on the simulated $E_{\rm p}$ evolution for each value of γ. The *purple* line indicates the time of peak flux of the simulated pulse. It is clear that the integrated $E_{\rm p}$ is correlated with the speed of the intrinsic spectral evolution but uncorrelated with the peak flux.

a function of the spectral evolution and has a value that is close to the maximum simulated $E_{\rm p}$. It is not correlated with the value of $E_{\rm p}$ at the time of peak flux. Additionally, the mean fitted $E_{\rm p}$ is calculated from the $\rm CC_{0.5}$ bins and compared to the integrated $E_{\rm p}$ which is systematically higher (see Table 1).

The integrated F_ν is calculated from the integrated fit and compared to the summed F_ν of the $\rm CC_{0.5}$. The integrated F_ν is systematically less that the summed F_ν. It is therefore difficult to make a connection between the time-resolved and time-integrated properties.

5.3 Reconstructing the Evolution of $E_{\rm p}$

Using the fits for each set of simulations, the time evolution of $E_{\rm p}$ is fit with a power law and the recovered temporal index is compared with the simulated value. In general, the various binning methods recover the simulated $E_{\rm p}$ evolution satisfactorily (see Table 2 and Figures 6, 7, and 8). There are, however noted exceptions.

		$\alpha = -1.$	$\alpha = 0.$
Binning	True γ	Fitted γ	Fitted γ
0.5s bins	1.0	1.18 ± 0.04	1.05 ± 0.02
1s bins		1.15 ± 0.04	1.04 ± 0.02
5s bins		1.29 ± 0.07	1.35 ± 0.03
Bayesian blocks		1.10 ± 0.04	1.03 ± 0.02
Knuth bins		0.99 ± 0.05	1.06 ± 0.02
S/N bins		0.81 ± 0.05	1.00 ± 0.02
0.5s bins	1.5	1.56 ± 0.05	1.50 ± 0.03
1s bins		1.57 ± 0.05	1.50 ± 0.03
5s bins		2.10 ± 0.09	2.07 ± 0.06
Bayesian blocks		1.57 ± 0.05	1.51 ± 0.03
Knuth bins		1.54 ± 0.05	1.49 ± 0.03
S/N bins		1.22 ± 0.08	1.47 ± 0.04
0.5s bins	2.0	1.98 ± 0.09	1.98 ± 0.04
1s bins		2.11 ± 0.10	1.96 ± 0.05
5s bins		2.99 ± 0.36	3.07 ± 0.14
Bayesian blocks		2.12 ± 0.11	1.97 ± 0.05
Knuth bins		1.95 ± 0.10	1.94 ± 0.04
S/N bins		1.73 ± 0.10	1.90 ± 0.05
0.5s bins	2.5	2.53 ± 0.12	2.32 ± 0.06
1s bins		2.41 ± 0.12	2.35 ± 0.07
5s bins		2.10 ± 0.16	3.07 ± 0.14
Bayesian blocks		2.49 ± 0.12	2.46 ± 0.07
Knuth bins		2.47 ± 0.14	2.36 ± 0.07
S/N bins		2.20 ± 0.16	2.37 ± 0.07

Table 2. The reconstruction of $E_{\rm p}$ evolution in time for the tested binning methods.

The bins produced by the S/N method systematically flatten the evolution of $E_{\rm p}$. The origin of the effect is difficult to ascertain. A subset of the simulated datasets were binned using a signal-to-noise ratio of 100 to check how the ratio affected the results. The reconstructed values of γ were all flattened compared to the simulated value. The fine time ($\rm CC_{0.5,1}$) bins both reconstructed the evolution well. On average, they steepened γ with some exceptions. The coarse ($\rm CC_5$) bins systematically steepened γ. Both the KB and BB methods are accurate in reconstructing the evolution with no exceptions. This may be due to the fact that they bin the data based on the inherent temporal structure of the lightcurve.

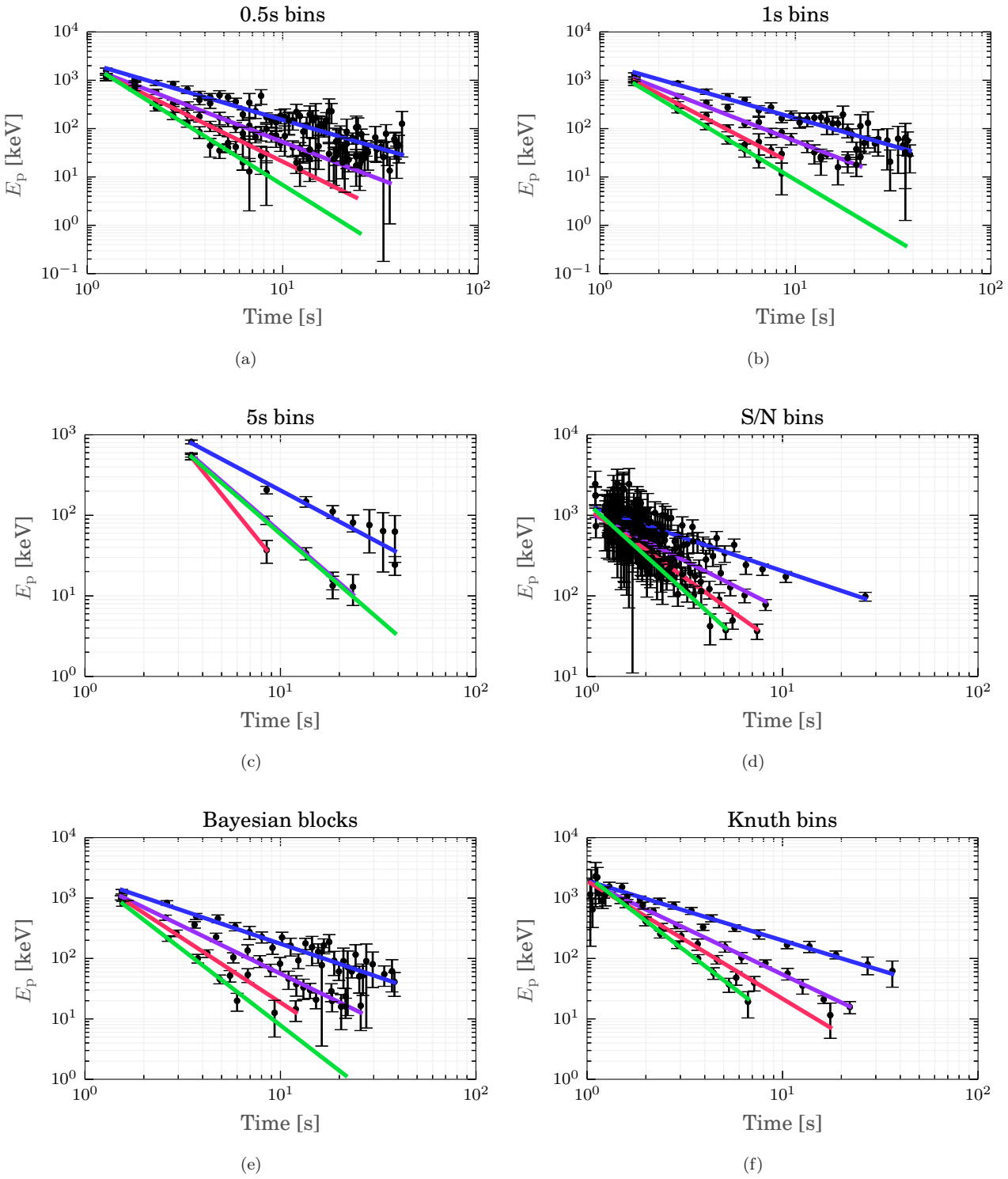

Figure 6. The reconstructed evolution of E_p for each of the binning methods with simulated $\alpha = -1$. The various fit lines indicate the reconstructed evolution for γ =1 (*blue*), 1.5 (*purple*), 2 (*pink*), and 2.5 (*green*). Some data points are missing due to the fitting engine failing to converge.

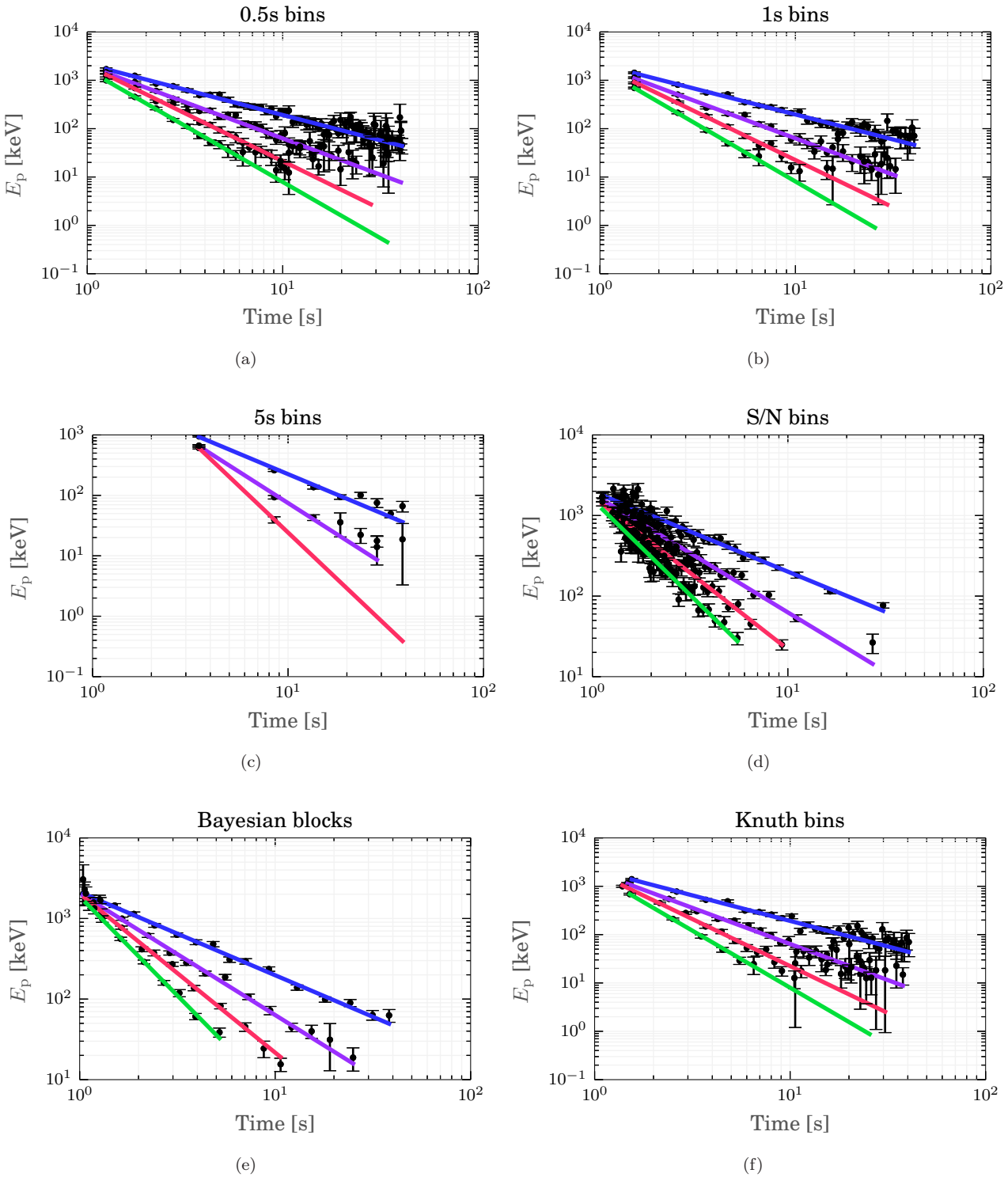

Figure 7. The reconstructed evolution of E_p for each of the binning methods with simulated $\alpha = 0$. The various fit lines indicate the reconstructed evolution for γ =1 (*blue*), 1.5 (*purple*), 2 (*pink*), and 2.5 (*green*). Some data points are missing due to the fitting engine failing to converge.

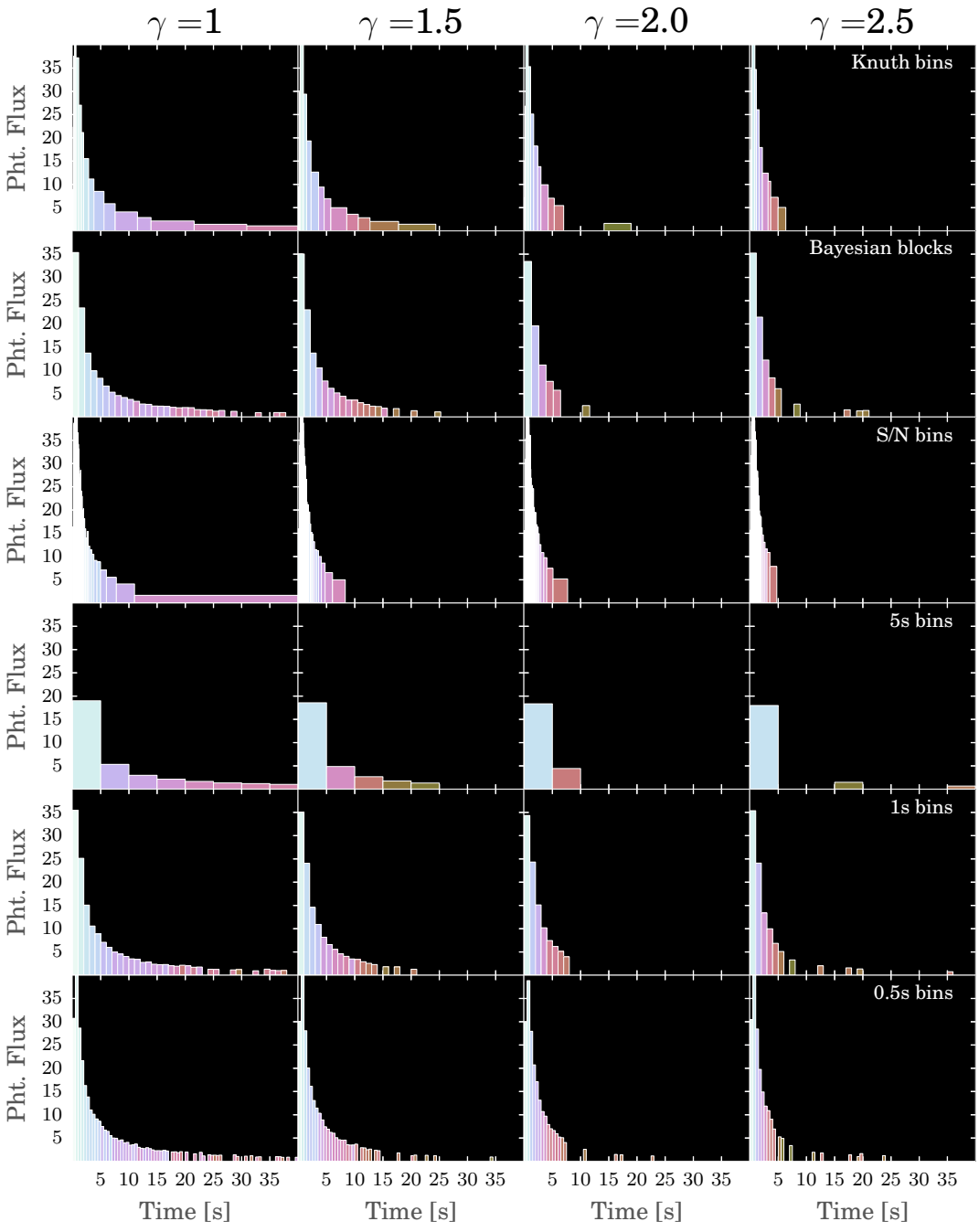

Figure 8. An example of the reconstructed flux and $E_{\rm p}$ from fits with $\alpha = -1$. Missing bins are due to the fitting engine failing to converge. It is obvious that coarse binnings have lower $E_{\rm p}$'s during the peak flux phase of the pulse. This is due to spectral averaging. When the evolution of $E_{\rm p}$ is fast ($\gamma = 2, 2.5$), it is difficult to fit spectral in the tail of the pulse because $E_{\rm p}$ quickly moves out of the instrument's bandpass. However, evolution this fast is rarely observed in GRBs. These plots can be compared to Figure 2 for the simulated $E_{\rm p}$ evolution.

α	Index	Integrated $E_{\rm p}$ [keV]	Average $E_{\rm p}$ [keV]	Integrated F_ν [erg s^{-1} cm^{-2}]	Summed F_ν [erg s^{-1} cm^{-2}]
-1	1.0	511.71	293.92	1.84e-06	1.38e-04
	1.5	725.27	369.33	1.33e-06	9.98e-05
	2.0	1091.00	436.71	1.13e-06	8.10e-05
	2.5	1127.36	487.78	9.50e-07	6.61e-05
0	1.0	867.36	241.88	4.17e-06	3.34e-04
	1.5	1127.91	347.39	2.90e-06	2.31e-04
	2.0	1349.98	405.60	2.23e-06	1.73e-04
	2.5	1296.32	482.99	1.88e-06	1.39e-04

Table 1. The integrated pulse properties of the simulated data set compared with the time-resolved properties.

5.4 Spectral Averaging

Spectral averaging occurs when the evolution of the spectrum across the duration of a time bin is summed. In the case of the Band function, with its adaptable fit parameters, the spectrum resulting from averaging its evolution across a time bin resembles a Band function. This may not be the case for actual physical models and therefore, it is pertinent to test how the spectral averaging of these models appears when fit with a Band function. Moreover, if the spectrum consist of multiple components that evolve in time independently as has been shown (Guiriec et al. 2011, 2013; Axelsson et al. 2012; Preece et al. 2014; Burgess et al. 2014), then fitting these time-averaged with the empirical Band function will give no physical insight into the models at all. Investigating the properties of physical model evolution is beyond the scope of this work. The focus here is on how time-averaging of the Band function affects the fitted values during data analysis.

The result of spectral averaging is apparent in Figure 8 where coarse time bins have a systematically lower $E_{\rm p}$ at the beginning of the pulse. The fitted value of $E_{\rm p}$ is compared with its simulated value in the center of the time bin in Figure 9. The most evident feature is that around the peak flux of the pulse, the S/N bins differ greatly from the simulated value. The coarse CC bins also differ greatly a late times in the pulse. While the overall evolution can be recovered in time, these differences become important when calculating physical parameters from the fit values.

Another interesting value to investigate is the Band function's low-energy index, α. This parameter is of interest because it is often used to interpret the type of high-energy emission that is occurring in the GRB jet (Baring & Braby 2004; Preece et al. 1998). While the value of α is held constant through out the simulated pulse, spectral averaging can affect its value in the fit. As seen in Figure 10, most binning methods reconstruct the value of α accurately except near the tail of the pulse where the flux is low. It is apparent that the S/N binning poorly reconstructs the value around the peak similar to what is observed with $E_{\rm p}$. Additionally, when the spectral evolution is very fast (γ=2,2.5), the recovered value of α systematically shifted to the softer values regardless of the binning method. This should be noted if it is found that $E_{\rm p}$ is evolving quickly in a GRB.

6 CONCLUSIONS

This investigation of the temporal binning of GRB lightcurves for spectral analysis has revealed several important factors to be considered when choosing time bins for spectral analysis. Coarse binning via the CC method of the data allows for a significant amount of counts to be used in the fit. This does not; however, imply that the fit is constrained or accurate. The differences of the fitted and simulated values of $E_{\rm p}$ with coarse binning can lead to incorrectly inferred physical values of the GRB jet. The overall trend of $E_{\rm p}$ can still be reconstructed with course binning but is unnecessary when the finer CC bins are more accurate at reconstructing $E_{\rm p}$. Still, the most accurate methods to bin the data are Knuth binning and Bayesian blocks. These methods take different approaches to determining the variability of the source but both are very accurate in reconstructing the values and evolution of $E_{\rm p}$. Both methods possess well prescribed reasoning for their form which can be used in justifying the methods use in spectral analysis.

The only methods that have negative effects on analysis is that of S/N bins and coarse CC bins. These bins poorly reconstruct both the evolution and values of $E_{\rm p}$. With S/N bins, the method is also not entirely objective. Bins of high flux are finer while bins of low flux are wide. This may not reflect either the intrinsic variability of the source or the underlying evolution of $E_{\rm p}$. Increasing the S/N ratio for a subset of the simulated dataset only furthered the problem. While it is possible that a value of S/N exists such that the correct evolution can be reconstructed, with real data there is no way to know what this correct value would be. It is entirely likely that such a value would change from burst to burst where temporally varying backgrounds and non-standard pulse shapes are common. Therefore, the method of using S/N to bin data is cautioned against when there are other methods that clearly give better results.

As mentioned above, none of these methods address a way to bin the data based on spectral evolution. The fact that KB and BB bins can accurately reconstruct the evolution of $E_{\rm p}$ and also have bins that are based on the intrinsic source variability points to these methods as an objective and accurate way to choose time bins. Both of these qualities are essential in identifying the physical emission processes and jet dynamics occurring in GRBs. Moreover, the observation that $E_{\rm p}$ is strongly correlated with energy flux in most GRBs further motivates the choice of a binning method that can select bins based upon the intrinsic flux evolution of the lightcurve. While the evolution simulated here is simple, it is a common evolution observed in GRBs. More complex evolutions may present problems for all methods.

Regarding the integrated properties of GRBs, based on this investigation it is difficult to infer meaning to the integrated $E_{\rm p}$ of a GRB without knowing the proper emission mechanism of the burst. This fact in combination with the studies of Kocevski (2012); Nakar & Piran (2005);

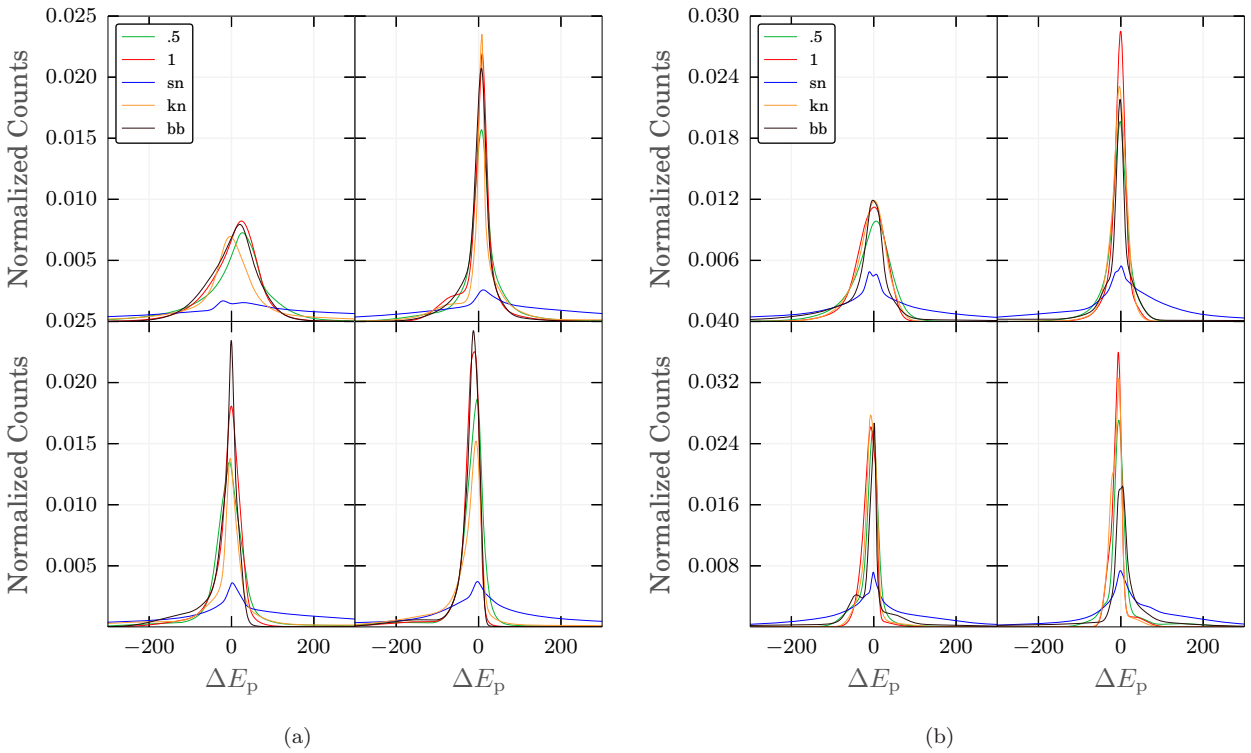

Figure 9. Continuous histograms of the shift of the fitted $E_{\rm p}$ from its simulated value. Clearly, the values obtained from S/N binning have a much larger spread than the other techniques. The fits made with Bayesian blocks have a better determination of $E_{\rm p}$ on average.

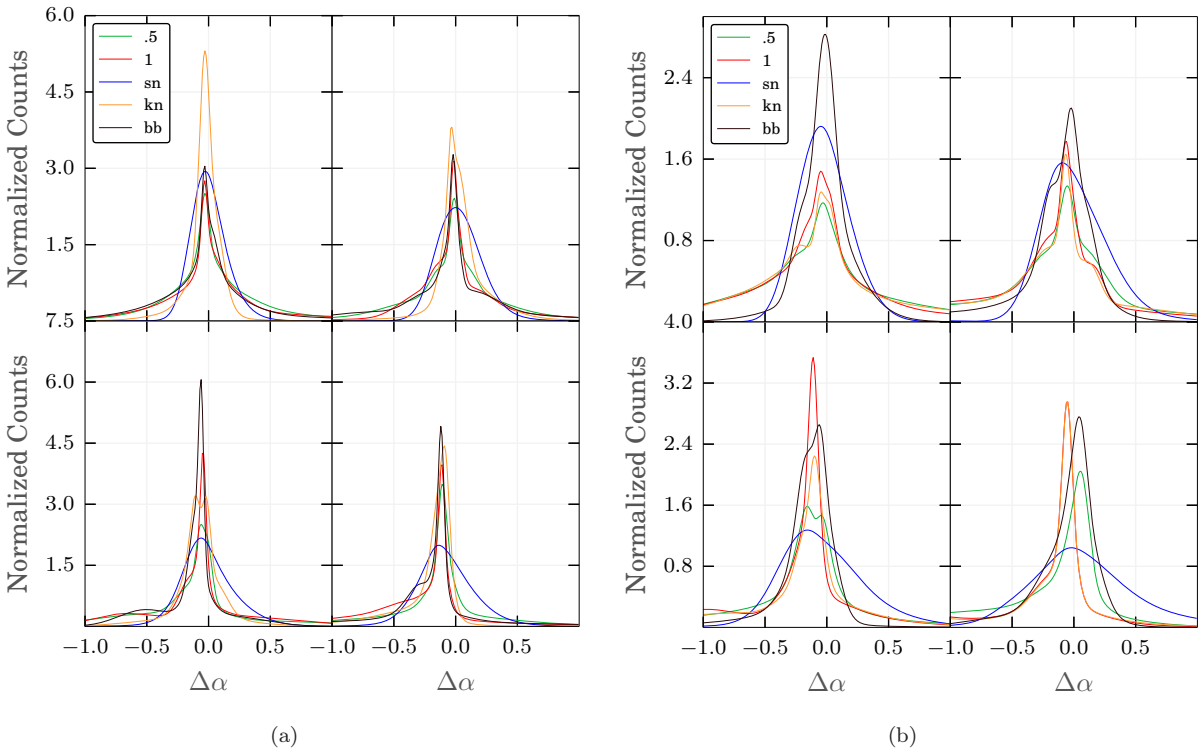

Figure 10. Continuous histograms of the shift of the fitted α from its simulated value. As with $E_{\rm p}$ (see Figure 9), the bins made with S/N have a much broader distribution and are less accurate than the other methods at reconstructing the true value of α.

Band & Preece (2005) make using the integrated properties of GRBs as cosmological tools difficult. If the proper emission mechanism is known, then the integrated spectra can be calculated from first principles and integrated fits will be useful for inferring physical properties. This is vitally important for examining short and/or weak GRBs which do not allow for time-resolved spectroscopy. Until this is accomplished, physical interpretations of integrated spectra should be done with extreme caution.

ACKNOWLEDGMENTS

JMB would like to thank Valerie Connaughton, Michael Briggs, Felix Ryde, and Rob Preece for useful discussions as well as the Oskar-Klein Center for supporting this work.

REFERENCES

Amati L., 2003, Chinese Journal of Astronomy and Astrophysics
Arnaud K., 1996, ASP Conf. Series, 101, 17
Axelsson M. et al., 2012, ApJL, 757, L31
Band D., Matteson J., Ford L., Schaefer B., 1993, ApJ
Band D., Preece R., 2005, ApJ
Band D. L., 1997, ApJ, 486, 928
Baring M. G., Braby M., 2004, ApJ
Burgess J. M. et al., 2014, ApJ, 784, 17
Crider A., Liang E., Preece R., Briggs M., Pendleton G., Band D., 1998, APS April Meeting Abstracts, -1
Ghirlanda G., Ghisellini G., Firmani C., 2005, MNRAS
Ghirlanda G., Ghisellini G., Lazzati D., 2004, ApJL
Goldstein A. et al., 2012, ApJS, 199, 19
Golenetskii S. V., Mazets E. P., Aptekar R. L., Ilinskii V. N., 1983, Nature, 306, 451
Guiriec S. et al., 2010, ApJ, 725, 225
Guiriec S. et al., 2011, ApJL, 727, L33
Guiriec S. et al., 2013, ApJ, 770, 32
Knuth K. H., 2006, arXiv.org, 5197
Kocevski D., 2012, ApJ, 747, 146
Kocevski D., Ryde F., Liang E., 2003, ApJ, 596, 389
Liang E., Kargatis V., 1996, Nature, 381, 49
Meegan C. et al., 2009, The Astrophysical Journal, 702, 791
Nakar E., Piran T., 2005, MNRASL, 360, L73
Norris J. P., Share G. H., Messina D. C., Dennis B. R., Desai U. D., Cline T. L., Matz S. M., Chupp E. L., 1986, ApJ, 301, 213
Preece R., Briggs M. S., Mallozzi R., Pendleton G. N., 1998, ApJL
Preece R. et al., 2014, Science, 343, 51
Scargle J. D., Norris J. P., Jackson B., Chiang J., 2013, ApJ, 764, 167
VanderPlas J., Connolly A. J., Ivezic Z., Gray A., 2012, 2012 Conference on Intelligent Data Understanding (CIDU), 47

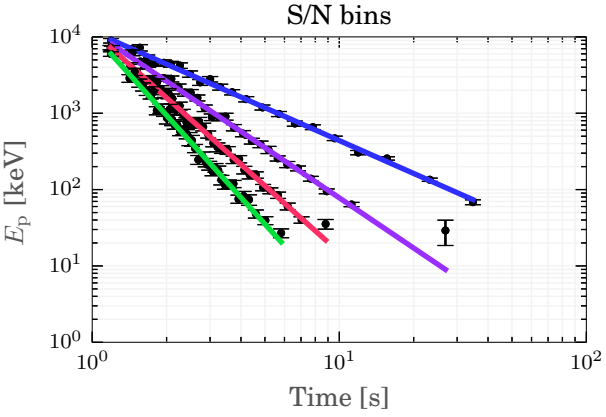
S/N bins
10^4
10^3
10^2
10^1
10^0
$E_{\rm p}$ [keV]
10^0
10^1
10^2
Time [s]